Development of power combination system for high-power and long-pulse ICRF heating in LHD

K. Saito[a], S.J. Wang[b], H.H. Wi[b], H.J. Kim[c], S. Kamio[a], G. Nomura[a], R. Seki[a,d], T. Seki[a], H. Kasahara[a], and T. Mutoh[e]

[a]*National Institute for Fusion Science, National Institutes of Natural Sciences, Toki, Gifu 509-5292, Japan*
[b]*National Fusion Research Institute, 169-148, Gwahak-ro, Yuseong-gu, Daejeon 34133, Korea*
[c]*ITER Organization, Route de Vinon-sur-Verdon, CS 90 046, 13067 St Paul Lez Durance Cedex, France*
[d]*SOKENDAI (The Graduate University for Advanced Studies), Department of Fusion Science, Toki, Gifu 509-5292, Japan*
[e]*Chubu University, Kasugai, Aichi 487-8501, Japan*

In the Large Helical Device (LHD), the development of high-power and long-pulse Ion Cyclotron Range of Frequencies (ICRF) heating system is ongoing. The developed Field-Aligned-Impedance-Transforming (FAIT) antenna has the potential for high-power injection of more than 1.8 MW. Here, to achieve this injection power, a power combination system was developed. An optimized power combiner was designed by repeated simulations, and then was fabricated and installed in the ICRF transmission system. Control of the power and the phase of incident waves into the input ports of the power combiner is important for the power combination. Therefore, a real-time control system was developed, and prompt reduction of power loss was demonstrated. As a result, combined powers of more than 2 MW for 6 s and 1 MW for 10 min were successfully achieved.

Keywords: ICRF heating; Power combination; FAIT antenna; LHD

1. Introduction

Ion Cyclotron Range of Frequencies (ICRF) heating is one of the reliable heating tools in the Large Helical Device (LHD) [1], and devices for high-power and long-pulse injection have been developed. The frequency of the ICRF heating was fixed at 38.47 MHz for the optimization of devices [2,3]. At this frequency, plasma is heated with the minority ion heating of hydrogen and the second harmonic heating of deuterium when the magnetic field strength on axis is around 2.75 T, which is standard in the LHD. It was previously clarified that the developed Field-Aligned-Impedance-Transforming (FAIT) antenna has a capability of power injection over 1.8 MW [3]. In order to reduce the voltage in the transmission line, the Ex-Vessel Impedance Transformer was also developed [4]. However, at this frequency, the output power of the transmitters in the LHD [5] is at most 1.2–1.3 MW for stable operation. In order to increase the power into the FAIT antenna, a power combination system is necessary.

Power combiners and power splitters, which have essentially the same structures, have been used for load-resilient RF injection into ELMy H-mode plasma in Tokamaks [6]. In the ASDEX Upgrade, the phase difference between two incident waves into the power combiner was automatically adjusted to 90° at high speed [7], and a wide band splitter was recently developed for ITER [8]. Here, we describe the development of a high-performance combiner for the LHD together with a control system that controls not only the phase difference but also the power of incident waves into the power combiner so as to minimize the power loss. As a result, power combination for high-power, long-pulse injection became possible.

In section 2, the design method and the performance of the fabricated power combiner are described together with the control system. In section 3, test results of the power combination are given. Section 4 summarizes the work.

2. Power combination system

Figure 1 shows a schematic view of the power combination system in the LHD. In this system a conventional power combiner with 4 ports was used. The frequency of ICRF heating is fixed at 38.47 MHz in the LHD, therefore, the power combiner was optimized at this frequency. In this figure the notations a_i and b_i express the incident and scattered waves at port i, respectively, and they have the following relation:

$$b_i = \sum_j S_{ij} a_j , \tag{1}$$

where S_{ij} is the component of the scattering matrix (S-matrix) of the power combiner. One of the output ports (port 4) is connected to the line where the reflection from the FAIT antenna is minimized with an impedance matching system [9]. The other port (port 2) is connected to the dummy load which can absorb MW-level power in continuous wave (CW) operation [5]. Input waves into port 1 and port 3 (a_1 and a_3) were automatically controlled using a phase shifter and attenuators inserted in the mW-level lines before the amplification by transmitters. The operating frequency is 38.47 MHz. However, harmonic

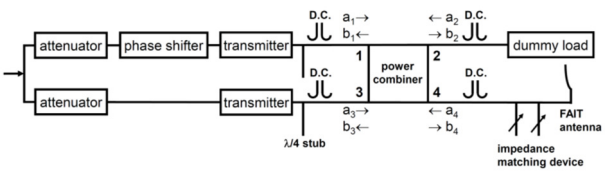

Fig. 1. Schematic view of power combination system. D.C. means directional coupler.

author's email: saito@nifs.ac.jp

waves are generated by the transmitters. In order to cut the second harmonic wave, which is the most intense harmonic wave, a short-ended stub with the length of a quarter wavelength was inserted at the outlet of the transmitter. The target combined powers of this system were set to 2 MW for high-power, short-pulse operation and 1 MW for steady-state operation.

2.1 Development of power combiner

(a) Design of the power combiner

Figure 2 shows the structure of the power combiner, which has input ports 1 and 3 and output ports 2 and 4. The inner diameter of the outer conductors is 203 mm and the outer diameter of the inner conductors is 88 mm—except for the center of the vertical lines, where the diameter is enlarged to 125 mm in order to reduce the characteristic impedance. The PTFE (polytetrafluoroethylene) spacers are attached at the flanges of the T-shaped junctions to support the inner conductors. All of the lengths between the junction points and the contact planes of flanges are 250 mm. Air ducts for the air cooling are attached for long-pulse operation. The power combiner was designed to fulfill the following three mandatory conditions.

1) Isolation
   Input ports 1 and 3 should be isolated to prevent direct power flow between the transmitters.
2) Impedance matching
   The reflected power from input ports 1 and 3 to transmitters should be zero when the reflected powers from the antenna and the dummy load are zero.
3) Power balance
   The input power into ports 1 and 3 should be the same.

Ideally, these conditions can be achieved with four quarter-wavelength transmission lines with the proper characteristic impedances. However, in an actual situation,

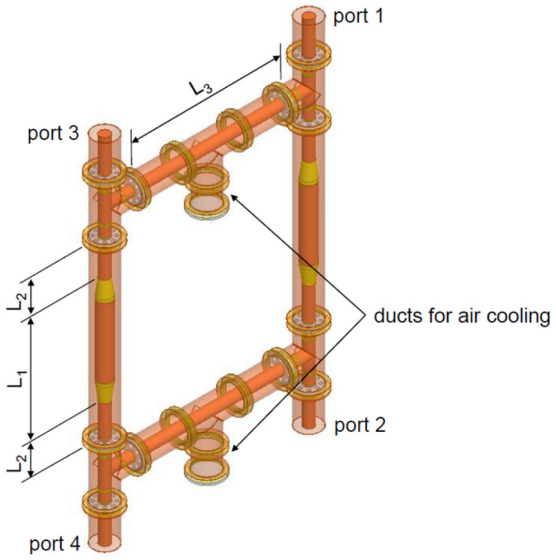

Fig. 2. Structure of the power combiner optimized with the adjustment of three parameters, L_1, L_2, and L_3. The converged values were 948.0 mm, 291.3 mm, and 1300.6 mm, respectively. Brown-colored parts are made of copper and yellow-colored parts are made of brass.

achievement of these conditions is difficult since there are several components with finite dimensions. Finite diameter of coaxial line distorts the electric field around the junction points. Moreover, ducts for air cooling with a finite diameter and PTFE spacers with finite thickness also cause the difference between electric and real lengths. Therefore, a simulation is necessary. The S-matrix of the power combiner is 4 by 4. However, by assuming the symmetry of the power combiner, the number of variables could be reduced to 4 as shown by the following equation:

$$S=\begin{pmatrix} S_{11} & S_{12} & S_{13} & S_{14} \\ S_{21} & S_{22} & S_{23} & S_{24} \\ S_{31} & S_{32} & S_{33} & S_{34} \\ S_{41} & S_{42} & S_{43} & S_{44} \end{pmatrix}=\begin{pmatrix} S_{11} & S_{12} & S_{13} & S_{14} \\ S_{12} & S_{11} & S_{14} & S_{13} \\ S_{13} & S_{14} & S_{11} & S_{12} \\ S_{14} & S_{13} & S_{12} & S_{11} \end{pmatrix}. \quad (2)$$

In the case of a non-dissipative system, the power is conserved for arbitrary incident waves. Therefore, the S-matrix is a unitary matrix and the following equation is obtained:

$$\begin{cases} |S_{11}|^2+|S_{12}|^2+|S_{13}|^2+|S_{14}|^2=1 \\ S_{12}^*S_{11}+S_{11}^*S_{12}+S_{14}^*S_{13}+S_{13}^*S_{14}=0 \\ S_{13}^*S_{11}+S_{14}^*S_{12}+S_{11}^*S_{13}+S_{12}^*S_{14}=0 \\ S_{14}^*S_{11}+S_{13}^*S_{12}+S_{12}^*S_{13}+S_{11}^*S_{14}=0. \end{cases} \quad (3)$$

When the condition of isolation is met, S_{13} is 0. Therefore, the following equations are derived:

$$\begin{cases} |S_{11}|^2+|S_{12}|^2+|S_{14}|^2=1 \\ \mathrm{Re}(S_{11}^*S_{12})=0 \\ \mathrm{Re}(S_{12}^*S_{14})=0 \\ \mathrm{Re}(S_{11}^*S_{14})=0. \end{cases} \quad (4)$$

The equation $\mathrm{Re}(A^*B)=0$ means that either A or B or both are 0, or they are orthogonal. In the complex plane, S_{11}, S_{12}, and S_{14} cannot all be orthogonal. Therefore, at least one of them must be 0. Since S_{12} and S_{14} cannot be 0 for the power combination, S_{11} is 0, i.e., the matching condition. It was also derived that the phase difference between S_{12} and S_{14} is 90°. On the other hand, from the matching condition, the isolation condition could be derived. Therefore, isolation is equivalent to impedance matching in the loss-less power combiner, and optimization was performed by considering only the isolation and power balance using the following equation:

$$\begin{cases} p_1=\mathrm{Re}(S_{13}) \\ p_2=\mathrm{Im}(S_{13}) \\ p_3=|S_{12}|-|S_{14}|. \end{cases} \quad (5)$$

Evaluation functions p_1, p_2, and p_3 must be 0. Though the matching condition (S_{11}=0) was omitted, this condition should be ascertained after the optimization since there is a power loss in the actual power combiner. As there are three evaluation functions, three design parameters (lengths in the power combiner) L_1, L_2, and L_3 are necessary for the optimization. The relation between the variations of evaluation functions and design parameters is written as

$$dp_i = \sum_j \frac{\partial p_i}{\partial L_j} dL_j . \quad (6)$$

With the above equation, the modification of design parameters was determined as follows:

$$\begin{pmatrix} \Delta L_1 \\ \Delta L_2 \\ \Delta L_3 \end{pmatrix} = - \begin{pmatrix} \frac{\partial p_1}{\partial L_1} & \frac{\partial p_1}{\partial L_2} & \frac{\partial p_1}{\partial L_3} \\ \frac{\partial p_2}{\partial L_1} & \frac{\partial p_2}{\partial L_2} & \frac{\partial p_2}{\partial L_3} \\ \frac{\partial p_3}{\partial L_1} & \frac{\partial p_3}{\partial L_2} & \frac{\partial p_3}{\partial L_3} \end{pmatrix}^{-1} \begin{pmatrix} p_1 \\ p_2 \\ p_3 \end{pmatrix}. \quad (7)$$

We adopted the lengths indicated in Fig. 2 as the design parameters. By iterating the simulation of the electromagnetic field using HFSS (High Frequency Structure Simulator, ANSYS), an optimized power combiner was designed. The simulated scattering matrix S is as follows:

$$S = \begin{pmatrix} (-65.8_{dB}, 122_{deg}) & (-3.02_{dB}, -142_{deg}) & (-88.1_{dB}, -106_{deg}) & (-3.02_{dB}, 128_{deg}) \\ (-3.02_{dB}, -142_{deg}) & (-65.4_{dB}, 121_{deg}) & (-3.02_{dB}, 128_{deg}) & (-84.3_{dB}, -155_{deg}) \\ (-88.1_{dB}, -106_{deg}) & (-3.02_{dB}, 128_{deg}) & (-66.6_{dB}, 115_{deg}) & (-3.02_{dB}, -142_{deg}) \\ (-3.02_{dB}, 128_{deg}) & (-84.3_{dB}, -155_{deg}) & (-3.02_{dB}, -142_{deg}) & (-66.3_{dB}, 126_{deg}) \end{pmatrix}. \quad (8)$$

The isolation and matching terms were less than -84.3 dB and -65.4 dB, respectively. The matching terms were not considered in the optimization, but they were sufficiently low. The condition of power balance was also fulfilled. Normally, the reflection from ICRF antenna is small since there are no strong ELMs in LHD. When the reflection is negligible, it was estimated from this matrix that the power loss by the combiner itself is only 0.22%. Moreover, it was clarified from the simulation that when the combined power is 2 MW, the maximum electric field is at most 7 kV/cm on the inner conductor at the PTFE spacers attached to the T-shaped junction near port 4. When the reflection from antenna side exists, at the worst phase of the reflection ratio, the maximum electric field will be multiplied by $1+|\Gamma_a|$, where Γ_a is the reflection ratio at the antenna side. It is also derived with the S-matrix that the absolute reflection ratio at the each transmitter side is the same with that of the antenna side.

(b) Measurement of the scattering matrix

The power combiner was fabricated and the scattering matrix was measured with a network analyzer as follows:

$$S = \begin{pmatrix} (-40.9_{dB}, 108_{deg}) & (-2.99_{dB}, -131_{deg}) & (-45.5_{dB}, 17.2_{deg}) & (-3.07_{dB}, 139_{deg}) \\ (-3.00_{dB}, -131_{deg}) & (-39.5_{dB}, 169_{deg}) & (-3.06_{dB}, 139_{deg}) & (-42.3_{dB}, 20.8_{deg}) \\ (-45.5_{dB}, 17.2_{deg}) & (-3.06_{dB}, 139_{deg}) & (-44.9_{dB}, -177_{deg}) & (-2.99_{dB}, -131_{deg}) \\ (-3.06_{dB}, 139_{deg}) & (-42.3_{dB}, 20.4_{deg}) & (-2.99_{dB}, -131_{deg}) & (-45.5_{dB}, 111_{deg}) \end{pmatrix}. \quad (9)$$

The isolation and matching terms were less than -42.3 dB and -39.5 dB, respectively, and higher than the values in the simulation but low enough to be used. The measured phases were different from the simulated phases since the port position in the measurement was different from that in the simulation. In the following control system, phases are defined at the junction points.

2.2 Development of the control system

Control of both the power and the phase of the incident waves into the input ports is important for the power combination in order to reduce the power loss into the dummy load. Therefore, a real-time control system was developed. There are directional couplers at the output ports of the transmitters. However, in order to eliminate the power loss at the dummy load perfectly, measurement of the wave into the dummy load b_2 is also necessary. Therefore, we attached directional couplers at the output ports 2 and 4 as shown in Fig. 1. The directional coupler at port 4 is used for the measurement of combined power and for the impedance matching. The two phase differences between the three waves into the input ports and the dummy load are measured. The three powers of these waves are also measured. For the control of the incident waves into ports 1 and 3, attenuators and phase shifter were set in a control unit together with the power and phase detectors. Moreover, a comparator and an RF switch for the instantaneous turning off of the RF were also installed in the control unit, in the case of the power into the dummy load exceeding the threshold. In order to cancel the wave into the dummy load connected to port 2, the following two methods were devised:

$$\text{Control method 1: } \begin{cases} \delta a_1 = -\sqrt{2} j b_2 \\ \delta a_3 = 0 \end{cases} \quad (10)$$

$$\text{Control method 2: } \begin{cases} \delta a_1 = -j b_2 / \sqrt{2} \\ \delta a_3 = b_2 / \sqrt{2} \end{cases} \quad (11)$$

where δa_1 and δa_3 indicate the supplemental values added to a_1 and a_3, respectively, for the adjustment. When control method 1 is utilized, b_2 is cancelled by the modification of a_1 keeping a_3 constant. When control method 2 is used, the injection wave into antenna b_4 is constant (δb_4=0). The data acquisition, calculation, and output of control voltages are performed with cRIO-9063 and IO modules produced by National Instruments. They were also installed in the control unit. Control voltages are adjusted gradually with several steps because the relation between input and output powers of transmitters is non-linear. The control is done in real-time during a shot and the initial control voltages are adjusted automatically between shots.

3. Results of the power combination tests

Testing of the power combination system was conducted in two steps. First, it was done with the power level of several mW without transmitters. After the controllability was confirmed, the power combination system was tested with the transmitters.

3.1 Test without transmitters

In this test, cables were connected to the 4 ports of the power combiner. Two output lines were terminated with 50 Ω terminators. Forward wave signals detected with directional couplers at each port were monitored with an oscilloscope. Figures 3(a) and (b) show the RF signals of the waves into port 1 and 3 and the waves from port 2 and 4 in the two control methods, which were obtained with the oscilloscope. Although the initial powers into ports 1 and 3 were the same, the initial phase difference between

these ports was set to 0°, which caused a power flow into both output ports. In both control methods, input waves were adjusted with a step time of less than 1 ms and the residual power from port 2 was successfully reduced to zero.

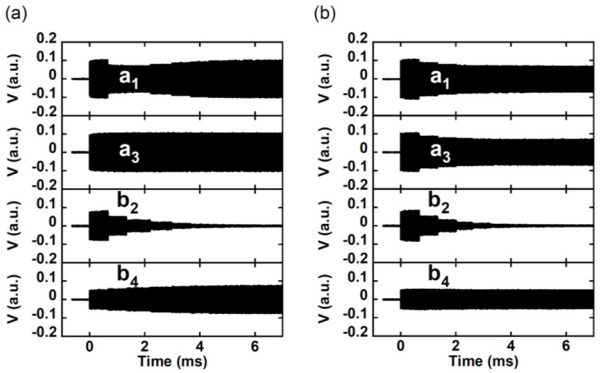

Fig. 3. Voltage of RF signals in the low power test with (a) control method 1 (constant port 3 power) and (b) control method 2 (constant port 4 power).

3.2 Test with transmitters

After the low-power test without transmitters, the power combiner was inserted into the transmission system. By using coaxial switches, port 2 was connected to the water-cooled small dummy load with the specification of CW 100 kW and port 4 to the large dummy load that can absorb power at a MW level in the CW operation. In this test, the large dummy load was used instead of the FAIT antenna. Two fans for the intake and the exhaust were attached to the air ducts in the power combiner for long-pulse operation. In the test with transmitters, control method 1 was used. Figures 4(a) and (b) show a comparison of the cases without and with control, where the experiments were conducted with moderate power. The initial control voltages for the phase shifter and attenuators were almost the same in the two cases. The control phase and gain in Figs. 4(a) and (b) indicate the relative phase shift and the relative gain of the control

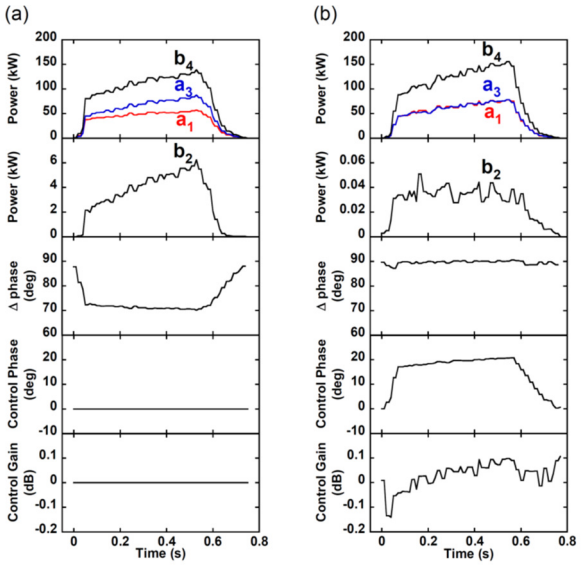

Fig. 4. Comparison between (a) without control and (b) with control.

devices for the incident wave into port 1, estimated from both control voltages applied to the phase shifter and the attenuator, and defined to be 0 in the case of without control as shown in Fig. 4(a). Although the reason is not known, the difference between the two input powers indicated by a_1 and a_3 gradually increased and the input phase difference Δphase (=phase(a_1)-phase(a_3)) deviated from 90° without control. As a result, the power into the small dummy load increased as shown in the second graph of Fig. 4(a). On the other hand, with control, the control phase and gain were modified automatically and the power into the small dummy load was successfully kept low, as shown in the second graph of Fig. 4(b). Then the two input powers indicated by a_1 and a_3 were almost the same and the input phase difference Δphase was maintained at around 90°. Figure 5(a) shows the results of the high-power experiment. Combined power of more than 2 MW lasted for 6 s. At the end of this shot, the combined power reached 2.3 MW. Figure 5(b) shows the results of the long-pulse experiment. The combined power of 1 MW lasted for 10 min. In each case, unwanted power loss at the small dummy load was kept sufficiently low, as shown in the second graphs of Figs. 5(a) and (b).

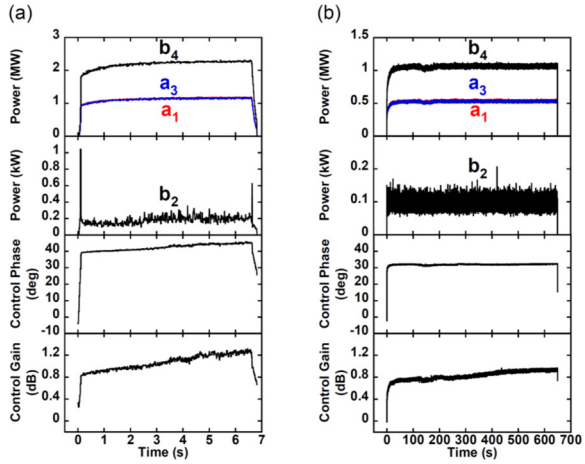

Fig. 5. Achievement of combined power of (a) over 2 MW for 6 s and (b) 1 MW for 10 min.

4. Summary

We developed a power combination system for ICRF heating with the FAIT antenna in the LHD. An optimized power combiner was designed and fabricated. It was confirmed with a network analyzer that two waves can be combined with almost perfect isolation and impedance matching. As a part of the power combination system, we also developed a control system, and prompt control of the two input waves was enabled. As a result, we successfully injected power of more than 2 MW for 6 s and 1 MW for 10 min into a dummy load.

Acknowledgments

The authors thank the LHD technical staff members for their contributions to this research. This research was financially supported by NIFS budget ULRR703.

References

[1] Y. Takeiri, T. Morisaki, M. Osakabe, M. Yokoyama, S. Sakakibara, et al., Nucl. Fusion 57 (2017) 102023.
[2] K. Saito, T. Seki, H. Kasahara, R. Seki, R. Kumazawa, et al., Fusion Eng. Des. 88 (2013) 1025-1029.
[3] K. Saito, T. Seki, H. Kasahara, R. Seki, S. Kamio, et al., Fusion Eng. Des. 96-97 (2015) 583-588.
[4] K. Saito, T. Seki, H. Kasahara, R. Seki, S. Kamio, et al., Journal of Physics: Conf. Series 823 (2017) 012007.
[5] T. Seki, R. Kumazawa, T. Mutoh, F. Shimpo, G. Nomura, et al., Fusion Sci. Technol., 40 (2001) 253-264.
[6] H. Faugel, P. Angene, W. Becker, F. Braun, V.V. Bobkov, et al., Fusion Eng. Des. 74 (2005) 319-324.
[7] D. Grine, F. Pompon, H. Faugel, H. Funfgelder, J.M. Noterdaeme, R. Koch, Radio Frequency Power in Plasmas AIP Conf. Proc. 1406 (2011) 105-108.
[8] H.J. Kim, S.J. Wang, B.H. Park, J.G. Kwak, J. Hillairet, J.J. Choi, Fusion Eng. Des. 96-97 (2015) 498-502.
[9] K. Saito, C. Takahashi, M. Yokota, G. Nomura, F. Shimpo, et al., Fusion Eng. Des. 83 (2008) 245-248.